Nonequilibrium Equation of State for Lennard-Jones Fluids and the Calculation of Strain-Rate Dependent Shear Viscosity

Alauddin Ahmed and Richard J. Sadus
Centre for Molecular Simulation, Swinburne University of Technology, Hawthorn, Victoria 3122, Australia

DOI 10.1002/aic.12257
Published online April 22, 2010 in Wiley Online Library (wileyonlinelibrary.com).

Nonequilibrium molecular dynamics simulation data for a 12-6 Lennard-Jones fluid are obtained over a wide range of temperatures, densities and strain-rates. The data, which cover 660 different state points, are used to deduce the nonequilibrium contributions to the energy and pressure of the fluid under steady-state conditions. These contributions are analysed and used in conjunction with an equilibrium equation of state to obtain an accurate nonequilibrium steady-state equation of state for the 12-6 Lennard-Jones fluid. Comparison with simulation data indicates that the nonequilibrium contributions can be obtained with a similar accuracy to the equilibrium contributions. Relationships for the shear viscosity as functions of density and pressure are obtained, which adequately reproduce the shear viscosity simulation data. The isochoric shear viscosity as a function of pressure is shown to be independent of strain-rate at sufficiently high strain-rates. © 2010 American Institute of Chemical Engineers *AIChE J,* 57: 250–258, 2011

Keywords: computer simulations (MC and MD), thermodynamics/statistical, rheology, liquids, nonequilibrium thermodynamics

Introduction

An equation of state typically provides an analytical relationship between the pressure (p), volume (V), temperature (T), and in the case of mixtures, composition (x) of a fluid. The prediction of fluid properties at thermodynamic equilibrium has been greatly facilitated by improvements in equations of state[1] that increasingly incorporate many of the underlying subtleties of intermolecular interactions. In particular, equations of state developed in conjunction with molecular simulation data[1] have proved valuable in predicting phenomena that are not easily experimentally accessible. However, many interesting thermodynamic processes[2,3] never attain thermodynamic equilibrium. Instead, some nonequilibrium phenomena, such as viscosity at constant shear rate,[4] eventually attain a nonequilibrium steady-state. This means that nonequilibrium thermodynamics is an important consideration for chemical engineering applications involving areas, such as rheology, lubricants, and confined fluids. Developing a reliable nonequilibrium equation of state is important for the prediction of such nonequilibrium processes.

Conventional equilibrium equations of state cannot be used for either nonequilibrium or nonequilibrium steady-state processes. However, it is feasible to formulate an equation of state specifically for nonequilibrium steady-states. Evans and Hanley[5–10] have used molecular simulation data to devise equations of state for both the pressure and energy of a steady-state fluid. In contrast to equations of state based on extended irreversible thermodynamics (EIT)[11] principles, which use a quadratic correction to the energy, these simulation-based equations use a strain-rate exponent of $\alpha = 3/2$.

Correspondence concerning this article should be addressed to R. J. Sadus at rsadus@swin.edu.au.

The $\alpha = 3/2$ exponent is consistent with both mode-coupling theory[9] and simulation data at the triple point of the 12-6 Lennard-Jones fluid. However, nonequilibrium molecular dynamics (NEMD) simulation data[12–14] for the pressure of a fluid under shear away from the triple-point indicates that the value of α varies continuously from 1.2 to 2 depending both on temperature and density.

In this work, we make use of this insight to formulate a steady-state equation of state for the pressure of a 12-6 Lennard-Jones fluid as a function of density, temperature, and strain-rate. NEMD simulations for shear viscosity are reported for a wide range of temperatures, densities and strain-rates. These extensive data are analysed to obtain the parameters of the equation of state. Pressure-strain-rate and density-strain-rate dependent relationships for shear viscosity are also reported and validated against simulation data.

Fundamentals

Simulation Details. The development of a nonequilibrium steady-state equation of state requires extensive simulation data for a wide range of state points. To obtain the required data, Gaussian thermostatted[4] NEMD simulations were carried out for 2048 12-6 Lennard-Jones particles. If we consider that a nonequilibrium stationary state of a fluid in Couette flow geometry is driven by an external shear rate the *sllod* equations[4] of motion are given by

$$\left.\begin{aligned} \dot{\boldsymbol{r}} &= \frac{\boldsymbol{p}}{m} + \boldsymbol{i}\dot{\gamma}\boldsymbol{r}_y \\ \dot{\boldsymbol{p}} &= \boldsymbol{F} - \boldsymbol{i}\dot{\gamma}p_y - \lambda\boldsymbol{p} \end{aligned}\right\} \tag{1}$$

In Eq. 1, m is the mass of the fluid; $\dot{\boldsymbol{r}}$ is the velocity; $\boldsymbol{p}$ is the peculiar momentum, which is the component of momentum in excess of that caused by the strain-rate; $\boldsymbol{i}$ is the unit vector in the x direction; $\dot{\gamma} = \partial v_x/\partial y$ is the strain-rate (v_x is the x-component of the streaming velocity), $\boldsymbol{F}$ is the intermolecular force and λ is the Gaussian thermostat given by $\lambda = \sum_{i=1}^{N} (\boldsymbol{F_i} \cdot \boldsymbol{p}_i - \dot{\gamma} p_{xi} p_{yi}) / \sum_{i=1}^{N} \boldsymbol{p}_i^2$. The total energy E and pressure tensor $\boldsymbol{P}$ in terms of peculiar momentum are obtained via:

$$E = \sum_{i=1}^{N} \frac{\boldsymbol{p}_i^2}{2\boldsymbol{m}} + \frac{1}{2}\sum_{i,j}^{N} \boldsymbol{u}_{ij} \tag{2}$$

$$\boldsymbol{P}V = \sum_{i=1}^{N} \frac{\boldsymbol{p}_i^2}{\boldsymbol{m}} - \frac{1}{2}\sum_{i,j}^{N} \boldsymbol{r}_{ij}\boldsymbol{F}_{ij} \tag{3}$$

where $\boldsymbol{r}_{ij} = \boldsymbol{r}_i - \boldsymbol{r}_j$, $\boldsymbol{F_{ij}}$ is the force on i because of j and u_{ij} is the intermolecular interaction energy between the particles. The second summation of the right hand side of Eq. 2 represents the configurational energy (E_{conf}).

The pressure was calculated as $p = 1/3Tr(\boldsymbol{P})$. The shear viscosity ($\eta$) was obtained from a component of the pressure tensor ($\boldsymbol{P}_{\text{xy}}$) and the strain-rate ($\dot{\gamma}$) via the relationship $\eta = -\boldsymbol{P}_{\text{xy}}/\dot{\gamma}$. Unless otherwise stated, all quantities in this work will be expressed in the conventional reduced form relative the depth (ε) and size (σ) Lennard-Jones parameters (i.e., $\rho^* = \rho\sigma^3$, $T^* = kT/\varepsilon$, $E^* = E/N\varepsilon$, $p^* = p\sigma^3/\varepsilon$, $\eta^* = \eta\sigma^2/\sqrt{m/\varepsilon}$, $\dot{\gamma}^* = \dot{\gamma}\sigma\sqrt{m/\varepsilon}$, $\tau^* = \tau\sqrt{\varepsilon/m\sigma^2}$). Hereafter, to simplify the notation all superscripts and the word reduced will be omitted from all quantities.

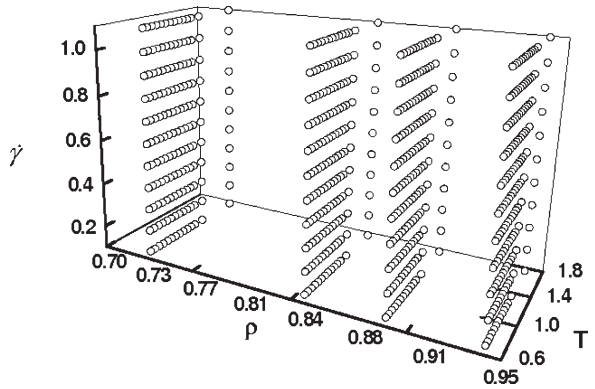

Figure 1. Illustration of the range of state points (ρ,T,$\dot{\gamma}$) for which NEMD simulations were performed to obtain data for the steady-state equation of state.

Data were obtained for a total of 660 state points.

The configurational energy per particle, pressure, and shear viscosity at different strain-rates were obtained for 660 different state points (Figure 1). This involved performing simulations at constant reduced densities of $\rho = 0.73$, 0.8442, 0.895 and 0.95 and a reduced temperature range $0.70 \le T \le 1.75$. At each density and temperature simulations were performed for 11 strain-rates rates that lie within $0.1 \le \dot{\gamma} \le 1.1$ at equal intervals of 0.1. The strain-rates were chosen to be well below the "string phase" region.[15]

The exponents and related coefficients [given below in Eq. 4] for both energy and pressure were previously[14] found to be independent of potential truncation. To save a significant amount of computational time, the simulations of the 660 state points were performed in a cubic box with a cut-off distance of 2.5σ. Lees-Edwards periodic boundary conditions were used.[4] The values of pressure and energy were accumulated without long-range corrections. The equations of motion were integrated with a five-value Gear predictor-corrector scheme[16,17] with a reduced integration time step of 0.001. A nonequilibrium simulation trajectory was typically run for 4×10^5 time steps. To equilibrate the system, the NEMD trajectory was first run without a shearing field. After the shearing field was switched on, the first 2×10^5 time steps of the trajectory were ignored and the fluid was allowed to relax to a nonequilibrium steady-state.

The statistical uncertainty in the results depends on the state point. It is particularly sensitive to the strain rate, with low strain-rates associated with larger errors than high strain-rates. Typically, the standard error in the reduced configurational energy is 10^{-5}–10^{-4}, compared with a 10^{-3}–10^{-2} error range for the reduced pressure. The range of standard errors in the reduced viscosity is typically 10^{-2}–10^{-1}.

Nonequilibrium Steady-State Equation of State. Following the approach reported by Evans and Hanley,[5] the pressure and the configurational energy (E_{conf}) at a given temperature, number density ($\rho = N/V$) and strain-rate can be obtained as the sum of equilibrium ($\dot{\gamma} = 0$) and nonequilibrium ($\dot{\gamma} > 0$) contributions:

$$\left.\begin{aligned} p(T,\rho,\dot{\gamma}) &= p_0(\rho,T) + p_{\dot{\gamma}}(\rho,T)\dot{\gamma}^{\alpha} \\ E_{\text{conf}}(T,\rho,\dot{\gamma}) &= E_{0\text{conf}}(\rho,T) + E_{\dot{\gamma}}(\rho,T)\dot{\gamma}^{\alpha} \end{aligned}\right\} \tag{4}$$

where the zero subscripts identify equilibrium properties.

The only difference between Eq. 4 and similar equations reported previously is that the α term replaces a fixed value of 3/2. Although it is tempting to refer to $p_{\dot\gamma}$ and $E_{\dot\gamma}$ as nonequilibrium "pressure" and "energy," terms respectively, it is evident that they do not have the corresponding dimensions for these quantities.

To obtain the value of α, we used the relationship reported by Ge et al.[14] from NEMD simulations of a 12-6 Lennard-Jones fluid:

$$\alpha(\rho,T) = a + bT - c\rho \tag{5}$$

where $a = 3.67 \pm 0.04$, $b = 0.69 \pm 0.03$ and $c = 3.35 \pm 0.03$. The parameterisation of Eq. 5 is valid[14] over a wide range of densities and temperatures. Although these parameters were obtained specifically for the 12-6 Lennard-Jones potential, there is some recent evidence[18] to suggest that they may be independent of the intermolecular potential. We note that theoretical considerations[19] require that the value of α should be less than 2.

To make use of Eq. 4, we need analytical relationships for the equilibrium contributions of the 12-6 Lennard-Jones potential. There are at least four[20–25] accurate expressions for the calculation of the equilibrium pressure for the 12-6 Lennard-Jones potential. The equilibrium pressure $p_0(T,\rho)$ can be obtained by fitting simulation data to the modified Benedict-Webb-Rubin (MBWR) equation proposed by Johnson et al.,[20] which is the most updated version of the equation of state first proposed by Nicolas et al.[25]

$$Z = 1 + \frac{1}{T}\sum_{i=1}^{8} A_i(T)\rho^i + \frac{\exp(-\delta\rho^2)}{T}\sum_{i=1}^{6} B_i(T)\rho^{2i} \tag{6}$$

where δ typically equals 3 and each of the A and B terms is the sum of multiple parameters.[25] This version of the equation of state accurately correlates pressure and internal energies from the triple point to about 4.5 times the critical temperature over the entire fluid range. The equilibrium configurational energy can be obtained from the following thermodynamic relationship:

$$E_{0\mathrm{conf}}(\rho,T) = \int_0^{\rho}\left(p - T\left(\frac{\partial p}{\partial T}\right)_{\rho}\right)\frac{d\rho}{\rho^2} \tag{7}$$

We calculated $E_{\dot\gamma}$ and $p_{\dot\gamma}$ by using Eq. 4 in conjunction with our simulation data for 660 state points (Figure 1). Values of $p_{\dot\gamma}$ and $E_{\dot\gamma}$ were determined using a least-squares fit of the sheared steady-state energy and pressure data obtained from the NEMD simulations.

It is convenient to introduce the following definition for the nonequilibrium steady-state compressibility factor:

$$Z_{\dot\gamma} = \frac{p_{\dot\gamma}\dot\gamma^{\alpha}}{\rho T} \tag{8}$$

It should be noted, that unlike its equilibrium counterpart when Eq. 8 is expressed in terms of real units $Z_{\dot\gamma}$ is not a dimensionless quantity. This relationship allows us to accurately fit our simulation data via the following polynomial[7]:

$$Z_{\dot\gamma} = X^m \sum_{i=0}^{3}\sum_{j=0}^{3} f_{ij}\dot\gamma^j \frac{X^i}{T^j} \tag{9}$$

where $X = \rho T^{-1/4}$. It has been reported[7] that this definition of X could be used to fit data for a soft sphere potential. Hanley and Evans[7] used a similar approach to fit their data for $\dot\gamma = 1$ and $\alpha = 2/3$. However, using $\dot\gamma = 1$ effectively means that neither $\dot\gamma$ nor α influenced the fit as 1 raised to any power remains unchanged. In contrast, our data covers values of $\dot\gamma$ from 0.1 to 1.1, and the value of alpha is not constant but varies as given by Eq. 5. Applying Eq. 9 to our data incorporates a strain-rate dependency in the fit.

Combining equilibrium and steady-state contributions via Eq. 4 means that the pressure of a nonequilibrium steady-state 12-6 Lennard-Jones fluid experiencing constant shear can be obtained from

$$p = \rho T + \sum_{i=1}^{8} A_i(T)\rho^{i+1} + \exp(-\delta\rho^2)\sum_{i=1}^{6} B_i(T)\rho^{2i+1} + \rho\sum_{i=0}^{3}\sum_{j=0}^{3} f_{ij}\dot\gamma^i X^{i+m} T^{1-j} \tag{10}$$

It should be noted that because Eq. 10 was obtained from fitting our simulation data it is free of any assumption concerning the thermodynamics of the nonequilibrium steady-state.

Relationships for Shear Viscosity. Non-Newtonian shear viscosity is usually studied as a function of strain-rate. However, for both real experiments and NEMD simulations the influence of temperature, density, and pressure are also significant. For example, McCabe et al.[26] have demonstrated qualitatively the pressure (or equivalently density) dependence of non-Newtonian viscosity for 9-octlyheptadecane. From NEMD simulation data they found that at high pressures 9-octlyheptadecane first showed shear thinning behavior at lower strain-rates.

To model viscosity, we first define a generic variable W that can represent T, ρ, p or $\dot\gamma$. Following the approach used by Kapoor and Dass,[27] we assume the ratio of the first and second derivatives of viscosity with respect to the compressibility factor is a W-independent parameter (Y).

$$Y = \left(\frac{\partial^2\eta(Z_{\dot\gamma},W)}{\partial Z_{\dot\gamma}^2}\right)_W \Bigg/ \left(\frac{\partial\eta(Z_{\dot\gamma},W)}{\partial Z_{\dot\gamma}}\right)_W \tag{11}$$

Successive integration gives

$$\left.\begin{aligned}\left(\frac{\partial\eta(Z_{\dot\gamma},W)}{\partial Z_{\dot\gamma}}\right)_W &= \eta'(0,W)\exp(YZ_{\dot\gamma})\\ \eta(Z_{\dot\gamma},W) &= \eta(0,W) + \frac{\eta'(0,W)\left(\exp(YZ_{\dot\gamma})-1\right)}{Y}\end{aligned}\right\} \tag{12}$$

Expanding the exponential and truncating after the first two terms leads, after simplification to:

$$\eta(Z_{\dot\gamma},W) = \eta(0,W) + \eta'(0,W)\left(Z_{\dot\gamma} + 0.5YZ_{\dot\gamma}^2\right) \tag{13}$$

Table 1. Values of p_0, $p_{\dot\gamma}$ and α Appearing in Eq. 4 for Three Different Densities and a Range of Temperatures

	$\rho = 0.73$			$\rho = 0.8442$			$\rho = 0.895$		
T	p_0	$p_{\dot\gamma}$	α	p_0	$p_{\dot\gamma}$	α	p_0	$p_{\dot\gamma}$	α
0.7	−0.384(3)	8.431(4)	1.985(2)	0.806(8)	9.49(1)	1.910(4)	1.95(1)	10.15(1)	1.853(5)
0.722	−0.301(3)	8.430(4)	1.981(2)	0.943(7)	9.479(9)	1.912(4)	2.12(1)	10.12(1)	1.859(5)
0.75	−0.182(3)	8.418(4)	1.983(2)	1.122(9)	9.44(1)	1.918(5)	2.32(1)	10.07(1)	1.863(6)
0.8	0.015(3)	8.401(4)	1.988(2)	1.431(6)	9.393(8)	1.925(3)	2.67(1)	10.01(1)	1.874(6)
0.85	0.209(3)	8.392(4)	1.981(2)	1.733(6)	9.353(7)	1.935(3)	3.02(1)	9.95(1)	1.883(6)
0.9	0.410(3)	8.372(4)	1.991(2)	2.028(4)	9.303(5)	1.937(2)	3.36(1)	9.89(1)	1.890(6)
0.95	0.604(3)	8.362(4)	1.989(2)	2.319(4)	9.271(5)	1.940(2)	3.71(1)	9.83(1)	1.901(6)
1	0.794(3)	8.355(4)	1.993(2)	2.609(4)	9.233(4)	1.949(2)	4.04(1)	9.78(1)	1.908(6)
1.05	0.988(3)	8.338(4)	1.994(2)	2.889(1)	9.203(1)	1.954(7)	4.36(1)	9.74(1)	1.912(6)
1.1	1.169(3)	8.330(4)	1.992(2)	3.164(3)	9.167(4)	1.954(2)	4.69(1)	9.69(1)	1.921(6)
1.15	1.351(3)	8.328(4)	1.990(2)	3.448(5)	9.141(7)	1.965(3)	5.01(1)	9.64(1)	1.927(6)
1.2	1.539(3)	8.311(4)	1.997(2)	3.718(3)	9.104(4)	1.966(2)	5.33(1)	9.59(1)	1.935(6)
1.25	1.710(3)	8.313(4)	1.990(2)	3.982(3)	9.086(4)	1.967(2)	5.64(1)	9.57(1)	1.935(6)
1.35	2.065(3)	8.295(4)	1.990(2)	4.501(3)	9.042(4)	1.968(2)	6.25(1)	9.49(1)	1.947(6)
1.75	3.421(3)	8.257(4)	2.001(2)	6.492(3)	8.910(3)	1.985(1)	8.58(1)	9.28(1)	1.974(6)

The values were obtained from a least-squares fit of NEMD simulation data for a range of strain-rates (detailed in the text). The statistical uncertainty in the last digit is given in brackets.

This means that the viscosity can be simply calculated from three adjustable parameter $\eta(0,W)$, $\eta'(0,W)$, and Y that can be easily obtained by fitting Eq. 13 to the simulation results. In the same way, we can obtain the viscosity as a function of pressure and strain-rate from:

$$\eta(p,\dot\gamma) = \eta(0,\dot\gamma) + \eta'(0,\dot\gamma)\left(p + 0.5Yp^2\right) \tag{14}$$

where, in this case Y is defined by:

$$Y = \left(\frac{\partial^2\eta(p,\dot\gamma)}{\partial p^2}\right)_{\dot\gamma} \Bigg/ \left(\frac{\partial\eta(p,\dot\gamma)}{\partial p}\right)_{\dot\gamma} \tag{15}$$

We can also obtain the viscosity as a function of density and strain-rate from:

$$\eta(\rho,\dot\gamma) = \eta(0,\dot\gamma) + \eta'(0,\dot\gamma)\left(\rho + 0.5Y\rho^2\right) \tag{16}$$

where, in this case Y is defined by:

$$Y = \left(\frac{\partial^2\eta(\rho,\dot\gamma)}{\partial\rho^2}\right)_{\dot\gamma} \Bigg/ \left(\frac{\partial\eta(\rho,\dot\gamma)}{\partial\rho}\right)_{\dot\gamma} \tag{17}$$

Results and Discussion

The state point and strain-rate coverage of our simulation data used to obtain nonequilibrium steady-state contributions is illustrated in Figure 1. The simulations were confined to the dense fluid region because at very low density neither energy nor pressure is strain-rate dependent. Equation 4 is valid for the entire fluid region with the exception of state points close to the freezing point. The pressure and energy data obtained by fitting the simulation data to Eq. 4 are summarized in Tables 1 and 2, respectively. It should be noted that the fits for energy and pressure should not be done independently.

A least-squares estimate of $p_{\dot\gamma}$ was obtained for each state point (ρ,T) over a range of strain-rates by using a multiple

Table 2. Values of $E_{0\text{conf}}$, $E_{\dot\gamma}$ and α Appearing in Eq. 4 for Three Different Densities and a Range of Temperatures

	$\rho = 0.73$			$\rho = 0.8442$			$\rho = 0.895$		
T	E_0	$E_{\dot\gamma}$	α	E_0	$E_{\dot\gamma}$	α	E_0	$E_{\dot\gamma}$	α
0.7	−4.9411(5)	0.1043(6)	1.59(2)	−5.6651(7)	0.2226(7)	1.256(9)	−5.933(1)	0.322(1)	1.08(1)
0.722	−4.9220(4)	0.1014(4)	1.58(1)	−5.6404(6)	0.2177(6)	1.259(8)	−5.903(1)	0.314(1)	1.09(1)
0.75	−4.8977(4)	0.0982(5)	1.61(2)	−5.6086(9)	0.212(1)	1.26(1)	−5.867(1)	0.305(1)	1.11(1)
0.8	−4.8579(7)	0.0941(8)	1.61(3)	−5.5515(6)	0.2006(6)	1.319(9)	−5.804(1)	0.293(1)	1.14(1)
0.85	−4.8169(4)	0.0888(5)	1.68(2)	−5.4971(4)	0.1924(5)	1.348(8)	−5.740(1)	0.279(1)	1.17(1)
0.9	−4.7783(4)	0.0855(5)	1.71(2)	−5.4432(7)	0.1830(8)	1.36(1)	−5.678(1)	0.266(1)	1.19(1)
0.95	−4.7783(4)	0.0855(5)	1.71(2)	−5.3912(8)	0.1758(9)	1.36(1)	−5.615(1)	0.253(1)	1.24(1)
1	−4.7028(3)	0.0787(4)	1.77(2)	−5.3379(7)	0.1674(7)	1.42(1)	−5.556(1)	0.243(1)	1.25(1)
1.05	−4.6659(4)	0.0753(4)	1.78(2)	−5.2868(4)	0.1616(5)	1.47(1)	−5.498(1)	0.234(1)	1.28(1)
1.1	−4.6303(5)	0.0736(6)	1.81(3)	−5.238(1)	0.155(1)	1.44(2)	−5.4397(6)	0.2246(6)	1.314(8)
1.15	−4.5952(4)	0.0712(4)	1.79(2)	−5.186(1)	0.148(1)	1.53(2)	−5.3807(8)	0.2146(8)	1.36(1)
1.2	−4.5606(4)	0.0691(4)	1.77(2)	−5.137(1)	0.142(1)	1.54(2)	−5.324(1)	0.205(1)	1.38(1)
1.25	−4.5258(4)	0.0677(5)	1.84(3)	−5.0895(7)	0.1383(8)	1.56(2)	−5.2697(6)	0.1995(6)	1.39(1)
1.35	−4.4577(4)	0.0628(5)	1.88(3)	−4.9946(5)	0.1288(6)	1.61(1)	−5.159(1)	0.183(1)	1.45(2)
1.75	−4.2012(4)	0.0538(5)	1.94(4)	−4.6353(4)	0.1021(5)	1.73(1)	−4.7463(9)	0.141(1)	1.61(2)

The values were obtained from a least-squares fit of NEMD simulation data for a range of strain-rates (detailed in the text). The statistical uncertainty in the last digit is given in brackets.

Table 3. Parameters for the Nonequilibrium Steady-State Equation of State Regressed from the Simulation Data of This Work

	$j = 0$	$j = 1$	$j = 2$	$j = 3$
f_{0j}	14.474498040195400	−6.647556155245270	3.917705698095090	−0.915316394378783
f_{1j}	−1.717513016301310	2.732677555831720	−0.446753567923021	−0.232780581631844
f_{2j}	6.717727912940890	−13.095727298095300	6.374714825509740	−0.834708529404541
f_{3j}	−7.343084320883140	15.874167538948800	−10.100511777914100	2.135496485879440
m	0.870890115604038			

non-linear Levenberg-Marquardt regression algorithm.[28] The *R-squared* value is 0.97, which indicates that we have accounted for almost all of the possible variability with the parameters given in the model. For each value of $p_{\dot\gamma}$ at a given T, ρ, and α (Table 1), several values of $Z_{\dot\gamma}$ can be obtained from Eq. 8 corresponding to different values of $\dot\gamma$. These data in turn can be accurately fitted to Eq. 9 using the coefficients summarized in Table 3. This means that Eq. 9 can be used over the entire range of densities, temperatures, and strain-rates studied (Figure 1). In contrast to our work, Evans and Hanly,[7] assigned a value of zero to several of the f_{ij} coefficients, which probably partly reflects the much more limited scope of their simulation data.

To check the validity of our fit we performed independent zero-shear rate equilibrium molecular dynamics simulations at a density of $\rho = 0.73$ and various temperatures. These simulation data are compared with the equilibrium pressure p_0 obtained from our least squares fit (Figure 2a). It is evident that the fit yields very good agreement with the simulation data. In most cases the relative deviation between the calculated and simulated equilibrium pressure is less than 2% (Figure 2b). The positive deviations in Figure 2b reflect the fact that the fit slightly over estimates the equilibrium pressure. In view of this, we can be confident that the estimates of $p_{\dot\gamma}, E_{\dot\gamma}$, and α are quite reasonable.

Figure 3 illustrates the variation of $p_{\dot\gamma}$ (Figure 3a) and $E_{\dot\gamma}$ (Figure 3b) as a function of temperature at various constant densities. It is apparent that both quantities progressively decline with increasing temperature. Increasing the density also increases the values of $p_{\dot\gamma}$ and $E_{\dot\gamma}$ for any given temperature. However, the effect of density is most noticeable at relatively low temperatures.

Figure 4a compares the steady-state compressibilities calculated at different strain-rates using Eq. 9 with simulation data at different temperatures. It is apparent that irrespective

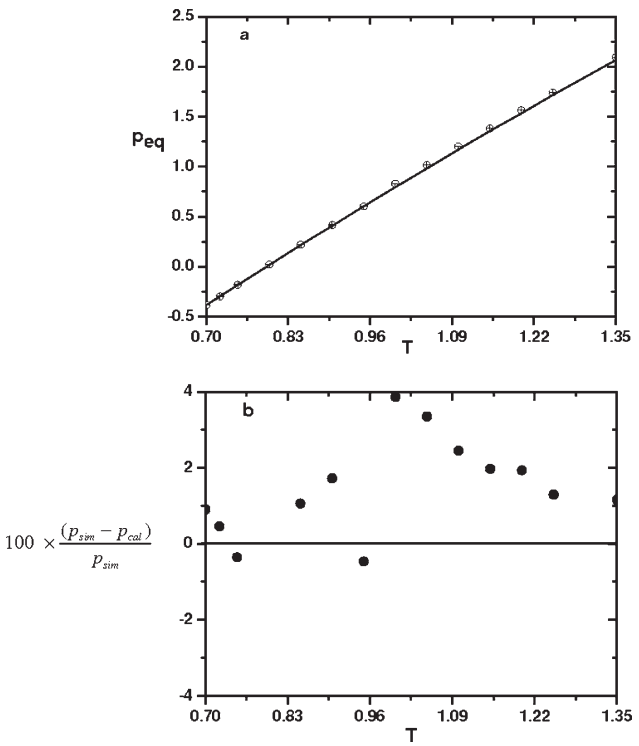

Figure 2. (a) Comparison of equilibrium molecular simulation pressure data (○) for Lennard-Jones fluid at $\rho = 0.73$ with values from Eq. 4 (solid line) and (b) the corresponding relative percentage difference (●).

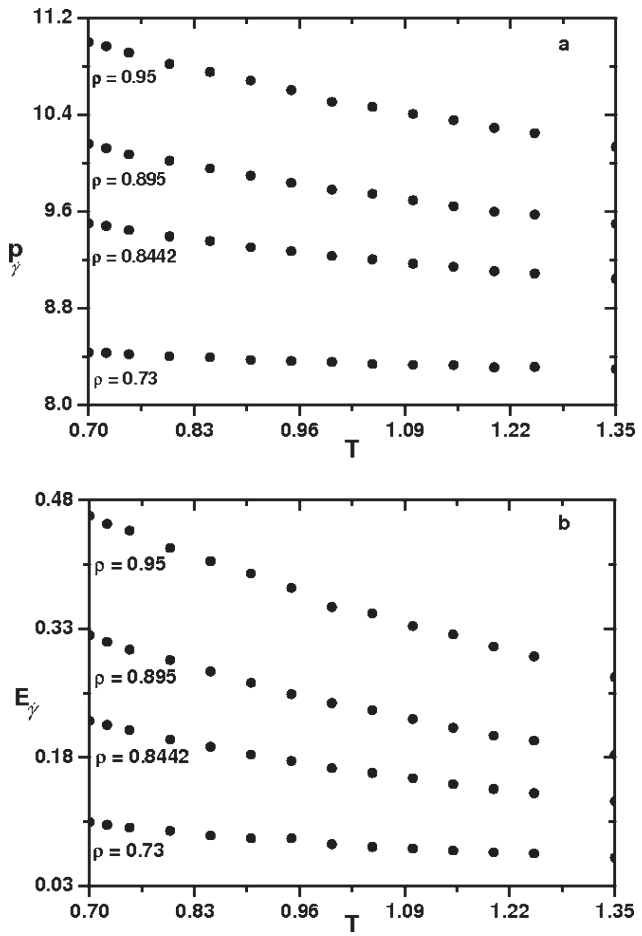

Figure 3. Nonequilibrium steady-state contributions to (a) $p_{\dot\gamma}$ and (b) $E_{\dot\gamma}$ for a Lennard-Jones fluid as a function of temperature at four different densities.

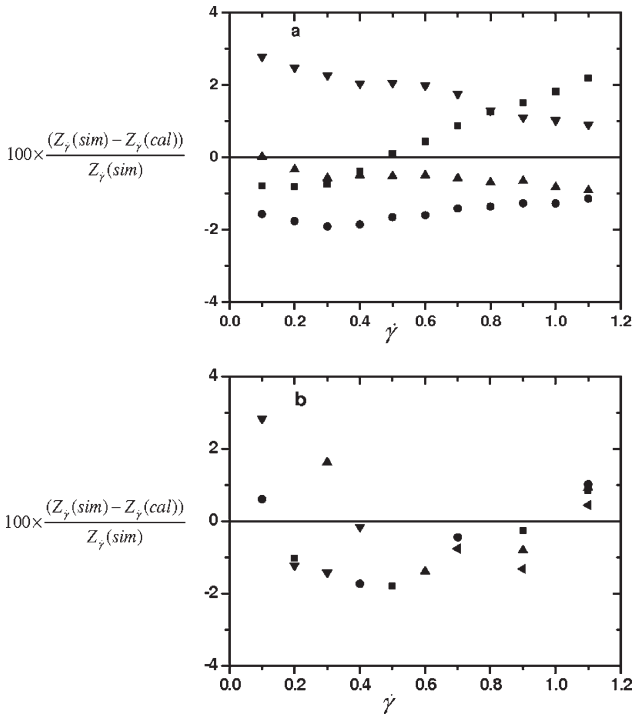

Figure 4. Comparison of the relative percentage difference of steady-state compressibility obtained from this work with the values calculated from Eq. 8 as a function of strain-rate (a) for the temperature range T = 0.70–1.75 and (b) for the density range 0.73–0.95.

Shown are (a) ρ = 0.73 (■), 0.8442 (●), 0.895 (▲), 0.95 (▼); (b) T = 0.7 (■), 0.90 (●), 1.10 (▲), 1.35 (▼), 175 (◀).

of either the strain-rate or the temperature, Eq. 9 can reproduce the simulation data to a typical accuracy of ~2%. A similar comparison for the accuracy of Eq. 9 with respect to both strain-rate and density is illustrated in Figure 4b. The quality of the agreement for density is similar to that observed for temperature.

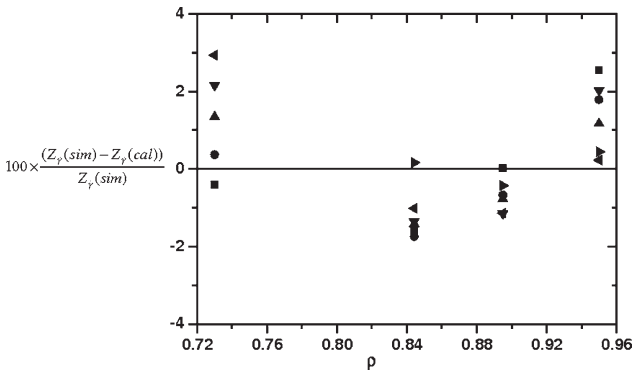

Figure 5. Comparison of the relative percentage difference of steady-state compressibility obtained from this work with the values calculated from Eq. 8 as a function of density.

Shown are $(T, \dot{\gamma})$ = (0.75, 0.1) (■); (0.90, 0.3)(●); (1.05, 0.5) (▲); (1.20, 0.7) (▼); (1.35, 0.9) (◀); (1.75,1.1) (▶).

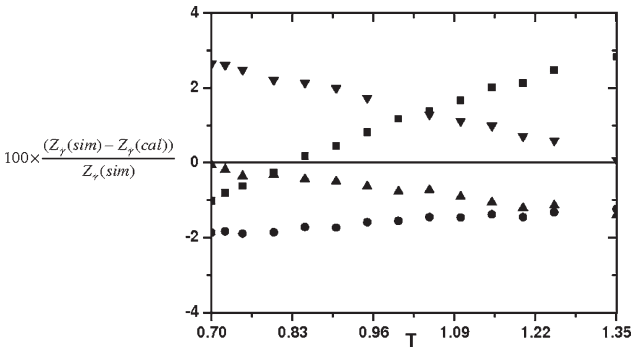

Figure 6. Comparison of the relative percentage difference of steady-state compressibility obtained from this work with the values calculated from Eq. 8 as a function of temperature.

Shown are $(\rho, \dot{\gamma})$ = (0.73, 0.2) (■); (0.8442, 0.4) (●); (0.895, 0.6) (▲); (0.95, 0.8) (▼).

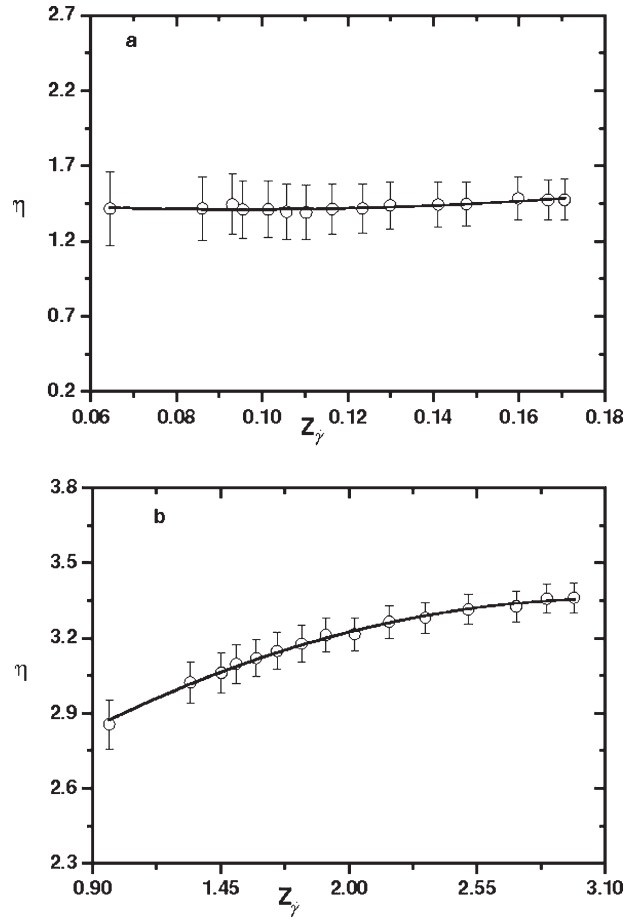

Figure 7. Shear viscosity for a 12-6 Lennard-Jones fluid as a function of nonequilibrium steady-state compressibility obtained from NEMD simulation (○) reported here and values obtained from Eq. 13 (solid lines) for T = 0.70 – 1.75 and (a) ρ = 0.73, $\dot{\gamma}$ = 0.1, (η(0,W) = 1.5242, η'(0,W) = −2.4179, Y = −10.5966) and (b) ρ = 0.895, $\dot{\gamma}$ = 0.4, (η(0,W) = 2.3128, η'(0,W) = 0.6770, Y = −0.3253).

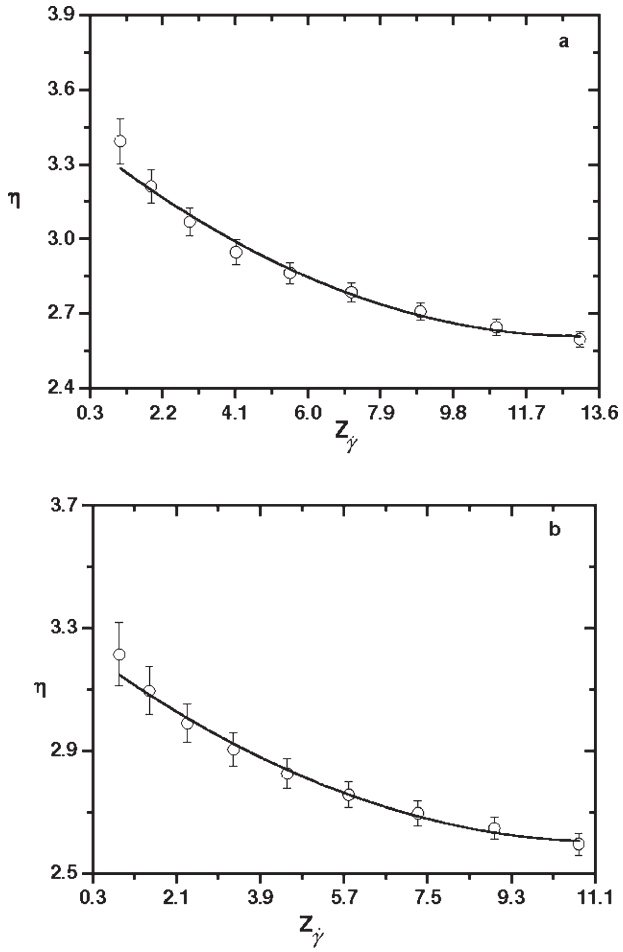

Figure 8. Comparison of the shear viscosity for a 12-6 Lennard-Jones fluid as a function of nonequilibrium steady-state compressibility obtained from NEMD simulations (○) at ρ = 0.8 reported here with values obtained from Eq. 13 (solid lines) for $\dot\gamma$ = 0.3–1.1 at (a) T = 1.0 (η(0,W) = 3.4143, η'(0,W) = −0.1224, Y = −0.0760) and (b) T = 1.20 (η(0,W) = 3.24193, η'(0,W) = −0.1120, Y = −0.0879).

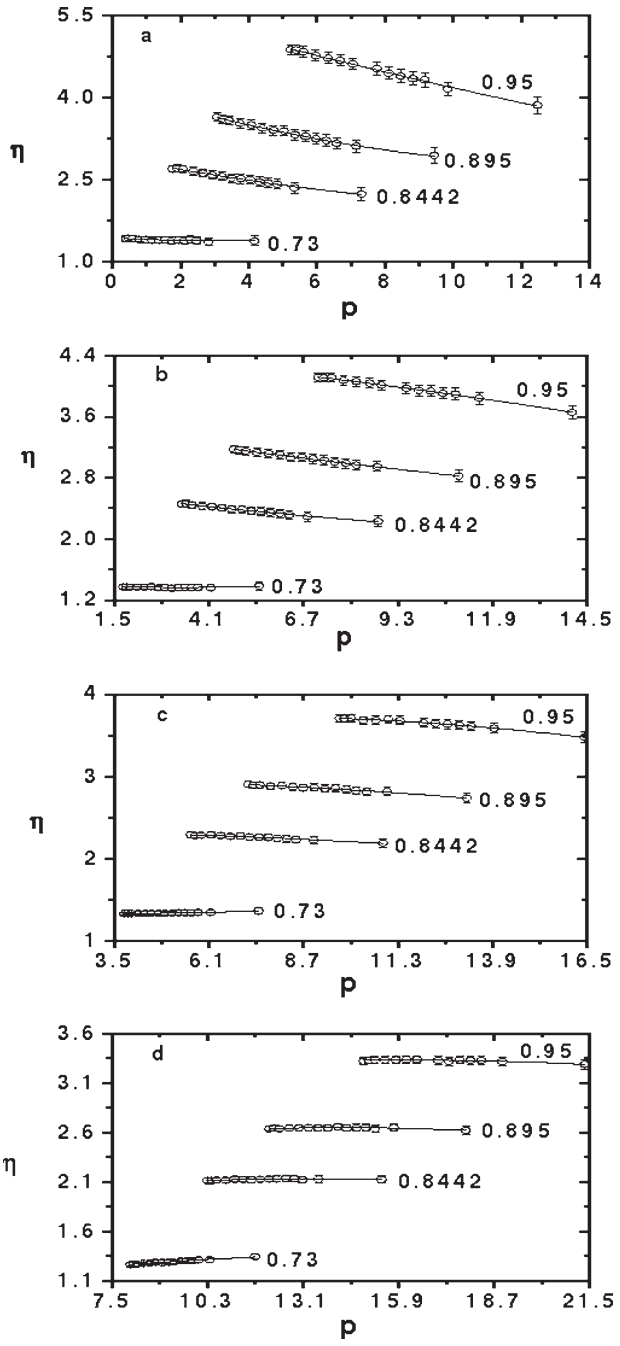

Figure 9. Comparison of shear viscosity simulation data (○) reported here for the 12-6 Lennard-Jones fluid as a function of pressure at four different densities and constant strain-rates of (a) 0.3 (η(0,$\dot\gamma$) = 1.4378, η'(0,$\dot\gamma$) = −0.0335, Y = −0.2925), (b) 0.5 (η(0,$\dot\gamma$) = 2.6617, η'(0, $\dot\gamma$) = −0.0653, Y = −0.0536), (c) 0.7 (η(0,$\dot\gamma$) = 2.9511, η'(0,$\dot\gamma$) = 0.0030, Y = −1.45) and (d) 1.0 (η(0,$\dot\gamma$) = 2.9294, η'(0,$\dot\gamma$) = 0.0499, Y = −0.0621) with values obtained from Eq. 14 (solid lines).

The data cover the temperature range of T = 0.70 to T = 1.75.

The accuracy of Eq. 9 for a given strain-rate and temperature at different densities is examined in Figure 5. At both low and high densities there is a tendency to overestimate $Z_{\dot\gamma}$, whereas the data is generally underestimated at intermediate densities. However, the error is small resulting in a relative deviation of ~2% in most cases. Figure 6 compares the ability of Eq. 9 to reproduce the compressibility data for a given strain-rate and density at various temperatures. For most temperatures the relative deviation is ~2%. Within this small error range, over estimates or under estimates appear equally likely, irrespective of the temperature.

The analysis presented in Figures 4, 5, and 6 clearly indicates that the steady-state equation of state can reproduce the simulation results over the range of densities, temperatures and strain-rates covered by this study. The quality of the fit for $Z_{\dot\gamma}$ is very close to the quality of agreement

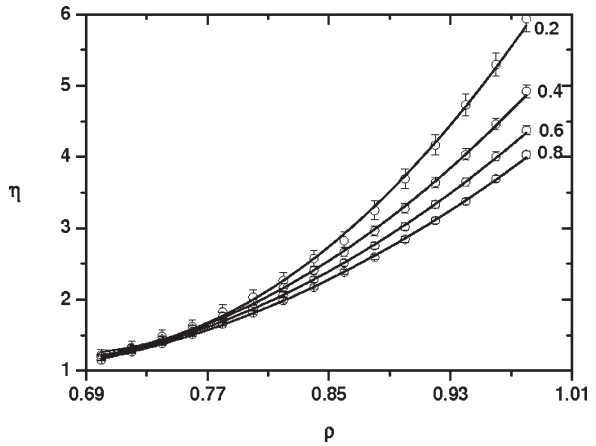

Figure 10. Comparison of shear viscosity simulation data (○) reported here for the 12-6 Lennard-Jones fluid at T = 1.0 as a function of density with values obtained from Eq. 16 (solid lines).

Results are shown for strain-rates of 0.2 ($\eta(0,\dot{\gamma}) = 25.9563$, $\eta'(0,\dot{\gamma}) = -72.1191$, Y = −1.4613), 0.4 ($\eta(0,\dot{\gamma}) = 15.0339$, $\eta'(0,\dot{\gamma}) = -43.1501$, Y = −1.5513), 0.6 ($\eta(0,\dot{\gamma}) = 10.7986$, $\eta'(0,\dot{\gamma}) = -31.5572$, Y = −1.6155) and 0.8 ($\eta(0,\dot{\gamma}) = 8.7105$, $\eta'(0,\dot{\gamma}) = -25.6701$, Y = −1.6591).

obtained for the pressure for the equilibrium 12-6 Lennard-Jones equation of state (see Fig. 4 in ref. 20). This means that we can expect the nonequilibrium equation of state to be of similar accuracy as its equilibrium counterpart.

The ability of Eq. 13 to reproduce our shear viscosity data is illustrated in Figure 7. The comparison, which involves both different densities and strain-rates, indicates that good agreement can be obtained for the full range of compressibility values. An analysis at a common density but different temperatures is given in Figure 8, which indicates that Eq. 13 can also accurately reproduce the temperature-dependence of shear viscosity.

Figure 9 compares the viscosity-pressure behavior obtained from Eq. 14 with simulation data at several different densities and strain-rates. We observe that it is rare for the shear-dependent viscosity to be investigated either experimentally or theoretically as a function of pressure. It is apparent that there is good agreement between Eq. 14 and the simulation data. From Figure 9 it can be observed that, irrespective of the strain-rate, the shear viscosity at a given pressure increases as the density is increased. For most densities, at low strain-rates, the shear viscosity declines noticeably as pressure is increased. However, as the strain-rate is increased, the rate of decline in the viscosity with respect to increasing pressure progressively decreases. This means that at a sufficiently high strain-rate, the shear viscosity is likely to be independent of pressure. However, the data at $\rho = 0.73$, which shows a small increase in shear viscosity with increasing pressure, appears to be an exception to this general behavior.

The variation of shear viscosity with respect to density at constant temperature is examined in Figure 10, which indicates that Eq. 16 can be used to reproduce the simulation data. The comparison involves data at different strain-rates. At low density, the shear viscosity is very similar irrespective of the strain-rate. However, a distinction in the shear viscosity begins to emerge at moderate density and increases progressively as the density is increased. At any moderate to high density, there is an inverse relationship between the shear viscosity and the strain-rate. That is, the shear viscosity decreases with increasing strain-rate.

It is apparent from the above comparisons that our shear viscosity model can accurately reproduce the simulation data. The most common method for reproducing strain-rate dependent shear viscosity data is to collapse the data onto a single characteristic curve.[29] It been demonstrated[30] this approach can yield a good qualitative representation between simulation and experimental data of the viscosity versus strain-rate behavior of squalane. The obvious disadvantage of this approach is that details of both pressure and temperature dependence of shear-viscosity are lost. To the best of our knowledge, accurate models for the strain-rate dependent shear viscosity, as functions of either pressure or density have not been reported. In contrast, as illustrated above, our approach accurately reproduces the simulation data for the shear viscosity with respect to both density and pressure. The agreement between our model and the simulation data is typically within an absolute average deviation (AAD) of less than 1%.

In addition to the comparison with simulation data, it would be highly desirable to compare our model with experimental data. In many cases, there are insufficient experimental data for strain-rate dependent shear viscosities at different temperatures, densities and pressures to obtain reliable values of the parameters of our model. Typically experimental measures focus on the effect of shear and as such they are conducted at a common pressure. In contrast, the shear viscosity of squalane has been reported[30] at different pressures and densities. We have compared our model with these simulation data in Figures 11 and 12. The comparison indicates that the model accurately reproduces the experimental viscosity-density and viscosity-pressure behavior of squalane.

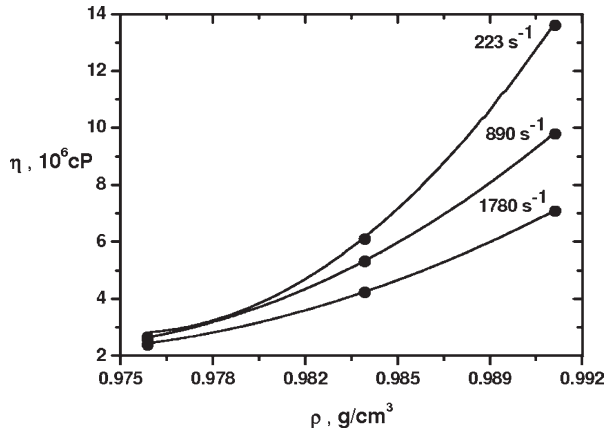

Figure 11. Comparison of experimental shear viscosities of squalane (●) at T = 20°C and various strain rates and densities with values obtained from Eq. 16 (solid lines).

Results are shown for strain-rates of 223 s^{-1} ($\eta\ (0,\dot{\gamma}) = 4.17 \times 10^{10}$ cPcm^3/g, $\eta'\ (0,\dot{\gamma}) = -8.55 \times 10^{10}$ cPcm^3/g, Y = −1.025 cm^3/g), 890s^{-1} ($\eta\ (0,\dot{\gamma}) = 1.92 \times 10^{10}$ cPcm^3/g, $\eta'\ (0,\dot{\gamma}) = -3.96 \times 10^{10}$ cPcm^3/g, Y= −1.029 cm^3/g) and 1780 s^{-1} ($\eta\ (0,\dot{\gamma}) = 1.14 \times 10^{10}$ cPcm^3/g, $\eta'\ (0,\dot{\gamma}) = -2.36 \times 10^{10}$ cPcm^3/g, Y = −1.03 cm^3/g). In all cases the AAD is less than 1%.

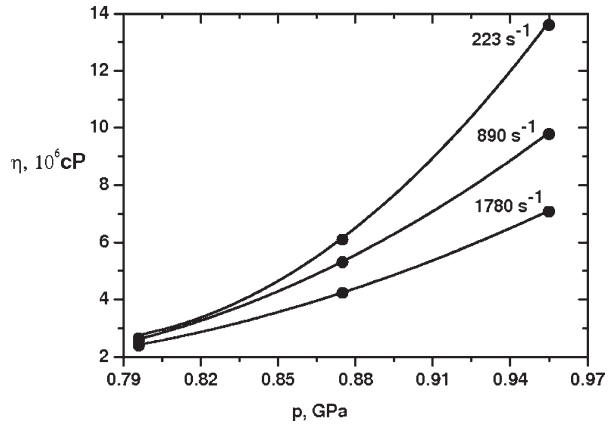

Figure 12. Comparison of experimental shear viscosities of squalane (●) at T = 20°C as a function of pressure with values obtained from Eq. 14 (solid lines).

Results are shown for strain-rates of 223 s^{-1} ($\eta(\mathbf{0},\dot{\gamma})$= 1.94 × 10^{17} cP/Pa, $\eta'(\mathbf{0},\dot{\gamma})$ = −4.99 × 10^{17}cP/Pa, Y = −1.3 × 10^{9} Pa^{-1}), 890 s^{-1} ($\eta(\mathbf{0},\dot{\gamma})$ = 7.13 × 10^{16}cP/Pa, $\eta'(\mathbf{0},\dot{\gamma})$ = −1.96 × 10^{17}cP/Pa, Y = −1.104 × 10^{9} Pa^{-1}) and 1780 s^{-1} (η $(0,\dot{\gamma})$ = 3.96 × 10^{16}cP/Pa, $\eta'(\mathbf{0},\dot{\gamma})$ = −1.10 × 10^{17}cP/Pa, Y = −1.448 × 10^{9} Pa^{-1}). In all case the AAD is less than 1%.

Conclusions

Extensive NEMD data for a 12-6 Lennard-Jones fluid have been obtained for a wide range of temperatures, density, and strain-rates, which can be used to deduce the nonequilibrium contributions to the energy and pressure of the fluid under steady-state conditions. The nonequilibrium compressibility factor can be accurately fitted to a polynomial function involving temperature, density, and strain-rate. Using this fit in conjunction with an equilibrium equation of state yields a nonequilibrium steady-state equation of state for the 12-6 Lennard-Jones potential. Comparison with simulation data indicates that the nonequilibrium contributions can be obtained with similar accuracy to the equilibrium contributions. Relationships for the shear viscosity as functions of density and pressure have been obtained, which adequately reproduce the simulation data. The isochoric shear viscosity as a function of pressure is shown to be independent of strain-rate at sufficiently high strain-rates.

Acknowledgments

Alauddin Ahmed thanks Swinburne University of Technology for a post-graduate scholarship. The Australian Partnership for Advanced Computing provided a generous allocation of computer time.

Literature Cited

1. Wei YS, Sadus RJ. Equations of state for the calculation of fluid-phase equilibria. *AIChE J*. 2000;46:169–196.
2. Jou J, Casas-Vázquez J, Lebon G. Extended irreversible thermodynamics. *Rep Prog Phys*. 1988;51:1105–1179.
3. Trepagnier EH, Jarzynski C, Ritort F, Crooks GE, Bustamante CJ, Liphardt J. Experimental test of Hatano and Sasa's nonequilibrium steady-state equality. *PNAS*. 2004;101:15038–15041.
4. Evans DJ, Morriss GP, *Statistical Mechanics of Nonequilibrium Liquids*, 2nd ed. London: Academic Press, 2008.
5. Evans DJ, Hanley HJM. Thermodynamics of steady homogeneous shear flow. *Phys Lett A*. 1980;80:175–177.
6. Evans DJ, Hanley HJM. Shear induced phase transitions in simple fluids. *Phys Lett A*. 1980;79:178–180.
7. Hanley HJM, Evans DJ. A thermodynamics for a system under shear. *J Chem Phys*. 1982;76:3225–3232.
8. Evans DJ. Computer "experiment" for nonlinear thermodynamics of Couette flow. *J Chem Phys*. 1983;78:3297–3302.
9. Evans DJ, Hanley HJM, Hess S. Non-Newtonian phenomena in simple fluids. *Phys Today*. 1984;37:26–33.
10. Romig KD Jr, Hanley HJM. Shear-induced phase changes in mixtures. *Int J Thermophys*. 1986;7:877–885.
11. Jou D, Casas-Vázquez J, Criado-Sancho M. *Thermodynamics of Fluids Under Flow*. Berlin: Springer-Verlag, 2001.
12. Marcelli G, Todd BD, Sadus RJ. Analytic dependence of the pressure and energy of an atomic fluid under shear. *Phys Rev E*. 2001;63:021204.
13. Ge J, Marcelli G, Todd BD, Sadus RJ. Energy and pressure of shearing fluids at different state points. *Phys Rev E*. 2001;64: 021201.
14. Ge J, Todd BD, Wu G, Sadus RJ. Scaling behavior for the pressure and energy of shearing fluids. *Phys Rev E*. 2003;67:061201.
15. Evans DJ, Morris GP. Shear Thickening and Turbulence in Simple Fluids. *Phys Rev Lett*. 1986;56:2172–2175.
16. Gear CW. *Numerical Initial Value Problems in Ordinary Differential Equations*. Englewood Cliffs, NJ: Prentice-Hall, 1971.
17. Sadus RJ. *Molecular Simulation of Fluids: Theory, Algorithms and Object-Orientation*. Amsterdam: Elsevier, 1999.
18. Desgranges C, Delhommelle J. Universal scaling law for energy and pressure in a shearing fluid. *Phys Rev E*. 2009;79:052201.
19. Evans DJ, Hoover WG, Failor BH, Moran B, Ladd AJC. Nonequilibrium molecular dynamics via Gauss's principle of least constraint. *Phys Rev A*. 1983;28:1016–1021.
20. Johnson JK, Zollweg JA, Gubbins KE. The Lennard-Jones equation of state revisited. *Mol Phys*. 1993;78:591–618.
21. Kolafa J, Nezbeda I. The Lennard-Jones fluid: an accurate analytic and theoretically-based equation of state. *Fluid Phase Equilibria*. 1994;100:1–34.
22. Chunxi L, Yigui L, Jiufang L. Investigation and improvement of equations of state for Lennard-Jones fluid. *Fluid Phase Equilibria*. 1997;127:71–81.
23. Adachi Y, Fijihara I. Generalized equation of state for Lennard-Jones fluids-I. Pure fluids and simple mixtures. *Fluid Phase Equilibria*. 1988;39:1–38.
24. Cuadros F, Mulero A, Okrasinski W, Ahumada W. An extensive study of the Helmholtz free energy of Lennard-Jones fluids using WCA theory. *Thermochimica Acta*. 1996;277:85–105.
25. Nicolas JJ, Gubbins KE, Street WB, Tildesley DJ. Equation of state for the Lennard-Jones fluid. *Mol Phys*. 1979;37:1429–1454.
26. McCabe C, Cui S, Cummings PT, Gordon PA, Saeger RB. Examining the rheology of 9-octylheptadecane to giga-pascal pressures. *J Chem Phys*. 2001;114:1887–1891.
27. Kapoor K, Dass N. A model for the pressure dependence of viscosity in liquids. *J Appl Phys*. 2005;98:066105–3.
28. Press WH, Teukolsky SA, Vetterling AWT, Flannery BP. *Numerical Recipes in C: The Art of Scientific Computing*. New York: Cambridge University Press, 1992.
29. Bird RB, Armstrong RC, Hassager O. *Dynamics of Polymeric Liquids: Fluid Mechanics*. New York: Wiley, 1987.
30. Bair S, McCabe C, Cummings PT. Comparison of nonequilibrium molecular dynamics with experimental measurements in the nonlinear shear-thinning regime. *Phys Rev Lett*. 2000;88:058302.

Manuscript received Feb. 2, 2010, and revision received Mar. 15, 2010.